Construction and Building Materials 374 (2023) 130816

Contents lists available at ScienceDirect

Construction and Building Materials

journal homepage: www.elsevier.com/locate/conbuildmat

Effects of amino acids on the multiscale properties of carbonated wollastonite composites

Rakibul I. Khan [a,b], Muhammad Intesarul Haque [a], Salman Siddique [a], Eric N. Landis [c], Warda Ashraf [a,*]

[a] Department of Civil Engineering, University of Texas at Arlington, Nedderman Hall, Arlington, TX 76010, USA
[b] Laticrete International, Inc., Bethany, CT 06524-3423, USA
[c] Department of Civil and Environmental Engineering, University of Maine, Orono 04473, USA

ARTICLE INFO

Keywords:
Calcium Silicate
Carbonation
$CaCO_3$
Biomineralization
Amino Acids
Wollastonite
Leaching
CO_2 footprint
Fracture toughness
Polymorphs

ABSTRACT

This article presents an insight into the effects of amino acids on the moisture susceptibility, nanomechanical properties, and fracture properties of carbonated wollastonite composites. Paste samples containing various concentrations of amino acids were subjected to a CO_2-rich environment. The addition of amino acids resulted in the formation of amorphous calcium carbonate (ACC), vaterite, and aragonite, instead of calcite, in the carbonated composites. Thermogravimetric analysis (TGA), Scanning electron microscopy (SEM), Fourier-transform infrared spectroscopy (FTIR), and nanoindentation were performed for microstructural analysis. Inductively coupled plasma-optical emission spectrometry (ICP-OES) was performed to determine the leaching of Ca^{2+} and Si^{2+} ions from carbonated wollastonite composites. It was observed that the chain lengths of the amino acids have an influence on the formation of crystal phases. For determining fracture properties, the Jenq-Shah model was performed using a notched beam. It was observed that amino acids reduced carbonation reaction and improved fracture properties by 156 %. The formation of metastable $CaCO_3$ enhanced the nanomechanical properties of this carbonated system.

1. Introduction

Concrete is the second most-consumed material annually after water [1,2]. According to the US Energy Information Administration (EIA), the traditional cement industries are the most energy-intensive manufacturing industries [3,4]. The conventional cement industry is responsible for 5–8 % of global CO_2 emissions to the environment [5,6]. The utilization of alternative cementitious materials instead of ordinary Portland cement (OPC) can substantially reduce the carbon footprint of the concrete industry. Therefore, several alternative cementitious systems with lower carbon footprint have been developed [7–14], among which carbonated low-lime calcium silicates (i.e., wollastonite) have gained recent popularity [15–23].

Wollastonite is a natural calcium silicate mineral with a crystalline needle structure [14,17,24]. It is a non-hydraulic mineral that reacts with CO_2 in the presence of water and produces $CaCO_3$ and Ca-modified silica gel. This $CaCO_3$ and Ca-modified silica gel act as binding phases and provide strength in this carbonated composite system [2,25,26]. During the carbonation curing, samples are kept in CO_2-rich environments. $CaCO_3$ has several polymorphs, including amorphous calcium carbonate (ACC), vaterite, aragonite, and calcite [27]. ACC, vaterite, and aragonite are metastable (addressed as $mCaCO_3$ in the remainder of this study) and are more soluble polymorphs of $CaCO_3$ compared to calcite [28]. For such a carbonation-activated system, the $CaCO_3$ polymorphs present in the sample affect these composites' strength and viscoelastic properties [13]. Prior research demonstrated that the crystalline characteristics of $CaCO_3$ govern the mechanical and microstructural performances of these carbonated cementitious composites [26,29–31].

By mimicking the biomineralization process, the stabilization of $CaCO_3$ polymorphs can be controlled [32]. In the biomineralization process, living organisms utilize various organic molecules to control the nucleation, polymorphic selection, and growth of $CaCO_3$ [33]. Specifically, L-Aspartic acid is one of such organic compounds that is efficient in controlling the $CaCO_3$ crystallization process [34]. Similar effects of L-Arginine and L-Serine have also been observed and are presented

* Corresponding author.
E-mail address: warda.ashraf@uta.edu (W. Ashraf).

https://doi.org/10.1016/j.conbuildmat.2023.130816
Received 10 July 2022; Received in revised form 16 February 2023; Accepted 19 February 2023
Available online 9 March 2023

elsewhere [32].

This study investigated the impact of these amino acids from nano to macro levels in the carbonation-activated wollastonite matrix. In addition to the multiscale characteristics, this study also investigated the role of amino acids on the ion-leaching characteristics of the carbonated wollastonite matrix. Leaching is a process of degradation consisting of the gradual dissolution of the cementitious matrix as a result of the migration of calcium ions and/ or silica ions to the pore solution. A higher amount of leaching significantly affects the strength of the cementitious composites [35] and degrades the material's mechanical and microstructural performances [36]. A recent study reported that the paste microstructure, rather than the matrix's calcium content, is mostly responsible for the resistance to leaching [37]. The matrix's microstructural homogeneity has a pivotal role in its resistance to leaching. Carbonated cementitious composites provide higher resistance to calcium leaching due to their refined pore structure [38,39]. Our previous study showed that adding amino acids stabilizes metastable $CaCO_3$ ($mCaCO_3$) polymorphs (i.e., vaterite and ACC) and refine the pore size distribution in the carbonated wollastonite matrix [32]. However, these $mCaCO_3$ polymorphs have high solubility constants [40,41], which can make the carbonated matrix susceptible to excessive leaching. Therefore, in this study, we evaluated the effects of amino acids on ions leaching from the carbonated wollastonite matrix.

To better understand the interaction between amino acids and carbonated matrix, the presented work investigated (i) the effects of amino acids on the carbonation reaction kinetics of wollastonite, (ii) the effects of amino acids on nanomechanical performances of carbonated wollastonite, (iii) leaching effects of carbonated matrix containing metastable $CaCO_3$ ($mCaCO_3$), and (iv) effects of $mCaCO_3$ on the fracture properties.

2. Materials and methods

2.1. Raw materials

The raw materials used in this study include commercially available ground wollastonite ($CaSiO_3$) (as a source of calcium silicate) and amino acids. Ground wollastonite was supplied by Nyco Minerals, USA, with a mean particle size of 9 μm and a specific surface area of 1.6 m^2/g. Fig. 1 and Table 1 show the particle size analysis and chemical composition of wollastonite. Details of this wollastonite can be found elsewhere [14,17]. Amino acids were purchased from VWR. Three types of amino acids were used in this study, including positively charged L- Arginine (L-Arg), less polar uncharged L-Serine (L-Ser), and negatively charged L-Aspartic (L-Asp).

2.2. Sample preparation

Powder amino acids were mixed with water at concentrations of 0.13 M and 0.25 M. Using the prepared amino acid solutions, Wollastonite powder was then combined to make paste samples with a solution-to-solid ratio of 0.42. The control batch was prepared by mixing wollastonite with deionized water without amino acid by maintaining the same solution-to-solid ratio. A total of seven batches (i.e., control, 0.13 M L-Arg, 0.25 M L-Arg, 0.13 M L-Ser, 0.25 M L-Ser, 0.13 M L-Asp, and 0.25 M L-Asp) were prepared for the nano to macro-level analysis.

Amino acid solution and wollastonite were hand-mixed for approximately 2 min. After mixing, 10–15 g of the paste was spread on a petri dish having a sample thickness of less than 2 mm, and this petri dish was then placed in a commercially available carbonation chamber (CO_2 incubator by VWR) where 80 % RH, and 20 % CO_2 concentration (atmospheric pressure) and 55 °C temperature was maintained. Compaction was avoided intentionally to reduce the diffusion effect of CO_2 across the sample. Carbonated paste samples were collected at regular intervals of 0.5, 3, 6, 10, 24, 72, 145, 200, and 300 h from the chamber. These samples were used for microstructural analysis. To eliminate uncertainty, three to four sample sets were carbonated and analyzed to verify the results. The variation in the results was less than 5 %.

Beam samples (40 mm × 30 mm × 180 mm) and disk samples (dia 25 mm, height 25 mm) were prepared using the paste mixture for fracture toughness and nanomechanical testing. Mixing was performed in a regular rotatory mixer for 2 min. After mixing, the paste samples

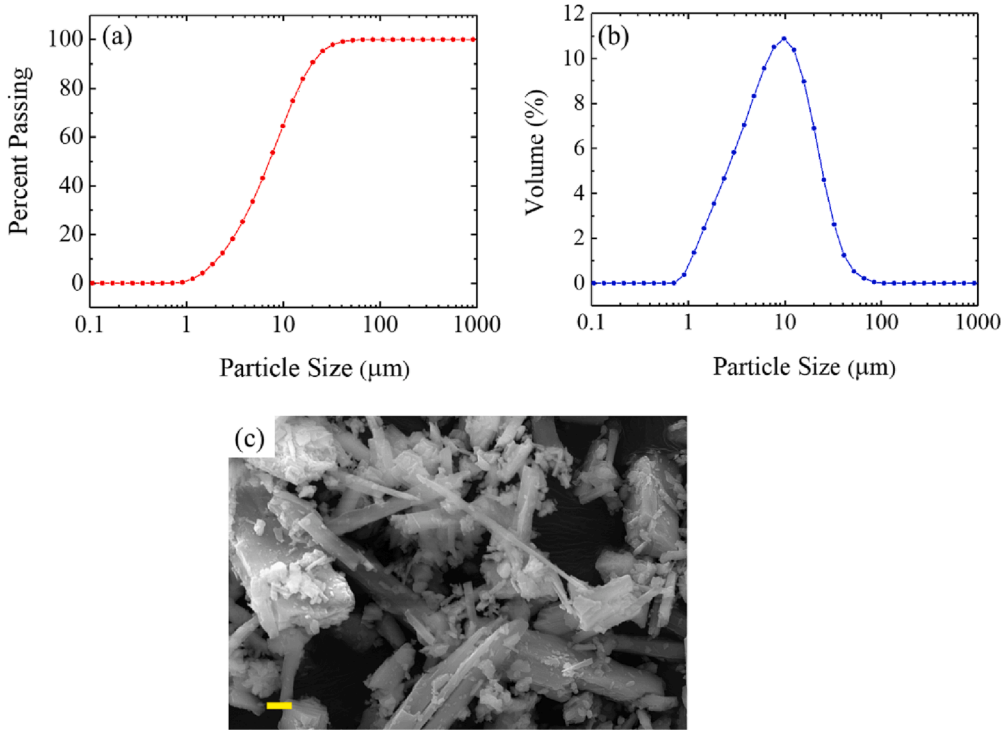

Fig. 1. (a), (b) Particle size distribution, and (c) SEM images of wollastonite ($CaSiO_3$). The scale bar shows a 2 μm distance.

Table 1
Composition of wollastonite.

	SiO_2	CaO	Al_2O_3	Fe_2O_3	MgO	SO_3	MnO	TiO_2
Wollastonite (weight %)	55.0	43.6	0.463	0.261	0.457	0.05	0.04	0.01

were compacted into beam molds in two layers and vibrated for a total of 30 s using a mechanical vibrator. Beam and disk samples were then kept in a carbonation chamber at 99.9 % of CO_2, 80 % RH, and 55 °C temperature. The beam and disk samples were demolded after 24 h of casting and were again placed in the CO_2 chamber for further carbonation curing until 145 h.

2.3. Experimental methods

2.3.1. Thermogravimetric analysis (TGA)

TGA was performed to determine the carbonation rate of wollastonite paste samples. A commercially available instrument (TA instrument, TGA 55) was used for this measurement. Approximately 30–40 mg powder sample was tested for each batch. The powdered sample was loaded into the Platinum pan and kept under isothermal condition for 5 min at 25 °C. The chamber temperature was then raised continuously to 980 °C with an increment of 10 °C per minute. Nitrogen gas was purged to ensure an inert environment. Initially, three replicate samples were tested through TGA for a few batches to validate for any deviation in carbonation across samples. The test result deviations were less than 2 % by weight of total carbonated samples.

$CaCO_3$ decomposes to CaO and CO_2 at around 400 ~ 800 °C [14,17,26,32,42]. To compare the effectiveness of different amino acids, the relative proportions of $CaCO_3$ polymorphs compared to the total carbonates formed in the matrix were determined by the ratio of 'weight loss from 400°C to 650°C' to 'weight loss from 400°C to 800°C.' The weight loss was calculated from 400°C (not from 200°C) to avoid the contribution from the evaporation of chemically-bound water, which occurs in the range of 200 to 350°C. Worthy of note, this approach underestimates the amount of $mCaCO_3$ (metastable $CaCO_3$) as these phases experience decarbonation in the entire range of 400°C to 800°C. The amount of $CaCO_3$ was calculated based on the following equation:

$$CaCO_3\,(\%) = (M_{400} - M_{800}) \times 2.27 \tag{1}$$

Where M_{400}, M_{800} are the masses (%) of the samples at the given temperatures.

After calculating $CaCO_3$, wollastonite's degree of carbonation (α) was determined using Eqn. (2) for the carbonation kinetics analysis.

$$Degree\ of\ carbonation, \alpha = \frac{Amount\ of\ CaCO_3(wt\%) at\ time\ t}{Maximum\ amount\ of\ CaCO_3(wt\%)\ formed\ in\ the\ control} \tag{2}$$

The carbonation kinetics procedure discussed in the previous research [43] was followed in this article. In general, the reaction kinetics of stage-1 carbonation reaction can be done using the 'geometric contraction model' [43], and stage-2, which is usually controlled by the diffusion of ions through the layer of the product formed during stage-1 follows a 'diffusion model' [44–46]. Both of these mechanisms can be represented using the following equation (Eqn. 3):

$$\left[1 - (1-\alpha)^{\frac{1}{3}}\right]^n = kt \tag{3}$$

Here 'k' is a reaction constant, 'α' is degree of carbonation, 't' is carbonation time, and 'n' is the reaction controlling factor. In this study, 'k' is a relative value, as the exact k-value depends on other experimental values such as particle size, and other properties. The reaction rate constants were evaluated through the logarithmic form of Eqn. 3 as shown in Eqn. 4.

$$\ln\left[1 - (1-\alpha)^{1/3}\right] = \frac{1}{n}\ln(k) + \frac{1}{n}\ln(t) \tag{4}$$

2.3.2. Scanning electron microscopy (SEM)

The tested beam samples were used to obtain SEM images on a Zeiss-FIB SEM instrument. The instrument was operated in high vacuum mode with a 5 kV accelerated voltage and a working distance of about 5 mm. The paste sample was Platinum (Pt)-coated before capturing SEM images.

2.3.3. Nanoindentation

Nanoindentation tests were performed on 145 h of carbonated disc paste samples. The discs were polished so that the surface became mirrorlike. The method of obtaining a mirrorlike shiny surface can be found elsewhere [47]. The load function had three segments: (i) loading from zero to maximum load in the span of 5 s, (ii) holding at the maximum load for 5 s, (iii) unloading from maximum to zero loads within 5 s. Since the depth of the indentations should also be small enough to determine the mechanical properties of the individual microscopic phases (i.e. indentation depth < characteristic size of each microscopic phase) [16], a maximum of 2500 μ-N force was selected for the SNI technique during this study. The average indentation depth for this load function was kept in the range of 100–300 nm for a 50 μ m × 50 μ m area. The elastic moduli were determined from the load-depth plots using the Oliver and Pharr method [48]. The experiment was performed using a Hysitron Triboindenter UB1 system (Hysitron Inc. Minneapolis, USA) fitted with a Berkovich diamond indenter probe. Throughout the test, a surface RMS roughness lower than 75 nm (measured with the Berkovich tip) was detected over an area of 50 μ m × 50 μ m.

2.3.4. Inductively coupled plasma-optical emission spectrometry (ICP-OES)

Inductively coupled plasma-optical emission spectrometry (ICP-OES) measurements were used to determine the leaching of Ca^{2+} and Si^{2+} ions. Beam samples carbonated for 145 h were used for this test. 100 g of sample from the tested beam were soaked in 400 g of deionized water for up to 48 h at 60 °C. The water to sample weight ratio was 4:1. After 6 h, 24 h, and 48 h, the samples were removed from the water, and the remaining water was filtered and tested for ICP-OES.

2.3.5. Fourier transform infrared spectroscopy (FTIR)

For identifying different polymorphs of $CaCO_3$, Fourier transformed infrared (FTIR) spectra were collected for the carbonated powdered sample using a Nicolet FTIR. The spectra were collected using the Attenuated Total Reflection (ATR) mode with 4 cm^{-1} resolution and 32 scans per sample. The signal to noise ratio was lower than 3:1.

2.3.6. Fracture toughness test

Notched beam tests determined the fracture properties and

toughness of the prepared carbonated beam samples. After carbonation for 145 h, a notch (one-third of beam depth) was made at the middle of the beam and tested in a closed-loop Instron machine with a displacement rate of 0.015 mm/min using a crack-mouth opening displacement (CMOD) control mode. Critical effective crack length, a_c was calculated based on the change between loading and unloading compliance [49,50]. In addition, the total work of fracture, or fracture energy, G_f, was evaluated by taking the area under the load-CMOD curves, less the unloading–reloading portion. We consider critical effective crack length as a measure of crack initiation toughness, while fracture energy is a measure of crack propagation toughness.

3. Results and discussions

3.1. Microscale effects of amino acids

3.1.1. Effects of amino acids on carbonation reactions kinetics

Calcite crystal formation and carbonation reaction can be controlled using different organic molecules [32,34,51–54]. During the carbonation reaction, calcium silicate reacts with CO_2 in the presence of water and forms calcium carbonate and Ca-modified silica gel. This carbonation reaction leads to the formation of $CaCO_3$, which exists primarily in the form of crystalline calcite. The present study investigated the effects of amino acids on the wollastonite carbonation reaction rate and the impact of amino acids on $CaCO_3$ polymorphs.

The amount of $CaCO_3$ content (by weight %) formed during carbonation is calculated using Eqn. 1 and is shown in Table 2. The formation of $CaCO_3$ was rapid initially (up to 10 h), and after that, there was a steadily growing stage (10 h to 300 h), as shown in Fig. 2. The quick dissolution of the calcium silicate phase could be the possible reason for this initial rapid carbonation reaction [2,43,46,55]. Following this rapid carbonation, the carbonation rate has reduced, and a slower reaction rate has occurred. This slow reaction rate lasted until the end of the exposed carbonation period (300 h). Initial rapid carbonation and later slow reaction could also be referred to as 'phase boundary control stage (stage 1)' and 'product layer diffusion stage (stage 2)', respectively [2,43,46,56]. The slower carbonation reaction rate after 10 h can be due to the lower diffusion of CO_2 into binder matrix caused by the formation of $CaCO_3$ layer.

As observed in Table 2, the carbonation rate in the wollastonite batch without amino acids was higher than that of amino acids batches. Thus, the amino acids' addition retarded the carbonation reaction of wollastonite. After 300 h of carbonation, wollastonite without amino acid produced ~ 30 % $CaCO_3$ (by weight), where 0.25 M concentration of L-Arg, L-Ser, and L-Asp acid mixed wollastonite produced 21 %, 19 %, and 16 % $CaCO_3$ by weight, respectively. L-Arg, L-Ser, and L-Asp acid of 0.13 M concentration mixed with wollastonite produced 21 %, 21 %, and 17 % of $CaCO_3$ (by weight) after 300 h of carbonation period. Based on these findings, it was revealed that a higher amount of amino acids reduced the carbonation rate (Table S1).

Eqn. 4 was plotted in Fig. 2 (b, c). For both stages, a good agreement was observed for theoretical values predicted by the model. For the ideal case, the slope of the fitted curves should be 1 for stage-1 and 0.5 for stage-2 [2,43]. In this study, for the control batch, the slope of the stage-1 curve was 0.83, and the slope for stage-2 was 0.13, which was close to the value predicted by a previous study [43].

The values of calculated reaction constants of stage-1 are shown in Fig. 3. The carbonation reaction rate was found to decrease with amino acids. Wollastonite without the addition of amino acid, has a higher carbonation rate, and wollastonite with the addition of L-Aspartic acid has the lowest carbonation rate.

The reduced amount of $CaCO_3$ formation and carbonation reaction rates of wollastonite, as observed in Fig. 2 and Fig. 3, respectively, can be attributed to the formation of metastable $CaCO_3$ ($mCaCO_3$) in the matrix. As reported in earlier research [32], the addition of amino acids increases the amount of ACC in the carbonated matrix. Due to ACC's high solubility, the formation of this phase results in the solution becomes saturated with Ca^{2+} and carbonate ions, thereby avoiding the additional dissolution of calcium silicate and CO_2 in the solution to react [57]. Consequently, the carbonation rate has been reduced [32–34]. Additionally, carboxylic groups ($COOH^-$) of amino acid have an unpaired electron that can bond with the Ca^{2+} ion in wollastonite. Amino acids can be adsorbed on the wollastonite surface as a result of this interaction, which reduces the amount of surface area accessible for the reaction [32]. Such a reduction in surface area is also attributed to a lower degree of carbonation. ACC is less denser than other polymorphs of $CaCO_3$ [58]. Thus, the higher amount of ACC leads to fewer pores in the carbonated matrix, resulting in low carbonation. Among the amino acids used in this study, L-Asp acid-containing carbonated wollastonite was found to have higher amounts of ACC than other amino acids [59], which subsequently resulted in lower $CaCO_3$ (by wt. %) formation in the composites (Fig. 2 (a)). Furthermore, the interaction between the organic additives and the surface of $CaCO_3$ particles can be considered to be governed by van der Waals force [60]. In suspension, the long alkly chain of additives prefer to adsorb on the surface of $CaCO_3$ rather than to hydrate with water retarding the dissolution. This interaction delays the phase transition of $CaCO_3$ by balancing the hydration energy, lattice enthalpy, and the surface energy of $CaCO_3$ particle [26,38,58,61–64].

3.1.2. Microstructural change due to amino acids

SEM images of carbonated composites after 145 h of carbonation are shown in Fig. 4, confirming the formation of metastable $CaCO_3$ in amino acid incorporated samples. Carbonation of the control batch formed calcite with a particle size greater than 2 μm (Fig. 4(a)). In the case of L-Arg, it reduced the size of the rhombohedral calcite crystal, as shown in Fig. 4(b). Fig. 4(c) shows the formation of plate shape vaterite in the case of L-Ser containing carbonated composites. L-Asp-containing carbonated composites formed a uniformly clustered amorphous $CaCO_3$ (ACC) with a particle size of less than 500 nm (Fig. 4(d)).

The addition of L-Arg resulted in the reduction of crystal size. The amino acids had a regulation effect on the crystal morphology of $CaCO_3$. It should be noted that along with the amino group, the carboxyl group in amino acids also plays an important role in controlling the morphology of $CaCO_3$. The limited growth of $CaCO_3$ can be due to the coordination of Ca^{2+} (from the partial dissolution of $CaCO_3$) with oxygen atoms of carboxyl group and nitrogen atoms. Due to this, the samples containing amino acids displayed smaller particle size than the control sample.

3.1.3. Nanomechanical properties

The disc samples were used to perform nanoindentation over two different 60 μm × 60 μm areas in a grid pattern. A total of 220 indentations were performed per paste sample. Fig. 5 shows the frequency distribution of the 145 h carbonated samples. The SNI (statistical nanoindentation) method was used to determine the mean elastic modulus of microstructural phases (i.e., Ca-modified silica gel, composite phase, hybrid phase, and calcite phase). In the control sample, it

Table 2
$CaCO_3$ content (% by weight) with carbonation duration.

Carbonation duration (hours)	Control	L-Arg		L-Ser		L-Asp	
		0.13 M	0.25 M	0.13 M	0.25 M	0.13 M	0.25 M
0.5	4.4	5.1	6.9	4.7	6.8	6.8	5.5
3	15.4	9.7	10.0	11.7	13.8	8.9	6.5
6	25.0	15.3	14.3	17.9	15.9	8.5	11.8
10	27.8	16.9	14.8	19.7	17.0	8.5	11.3
24	29.0	17.9	16.5	20.5	17.8	9.4	12.4
72	29.3	19.6	18.2	20.8	19.2	10.6	12.3
145	29.5	20.5	18.9	21.0	18.4	12.4	12.7
200	29.4	20.8	20.3	21.2	18.4	14.0	13.5
300	29.5	20.9	21.0	21.2	18.8	17.4	16.4

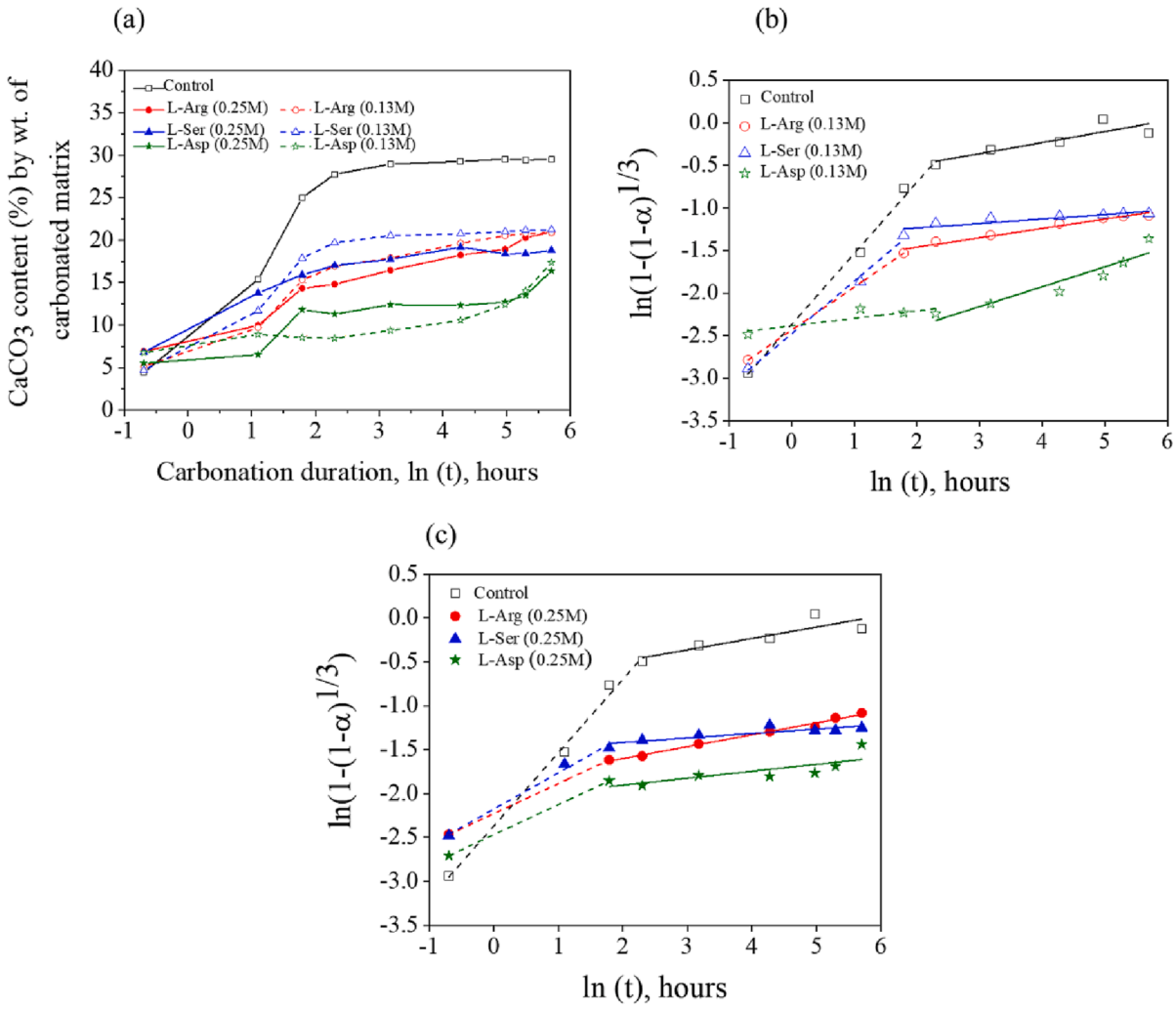

Fig. 2. (a) $CaCO_3$ content (% by weight) vs ln(t), (b, c) representing the predicated model (lines) and actual (data points) values of $ln[1-(1-\alpha)^{1/3}]$ vs ln(t) for carbonation kinetics of various amino acid batches, (b) 0.13 M, and (c) 0.25 M concentration. Dashed lines represent stage-1 and solid lines represent stage-2 carbonation reaction, respectively.

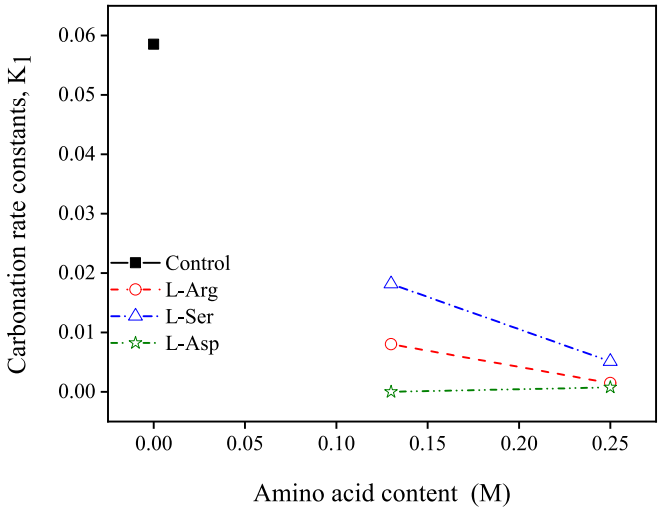

Fig. 3. Carbonation reaction rate constants of 'stage 1'.

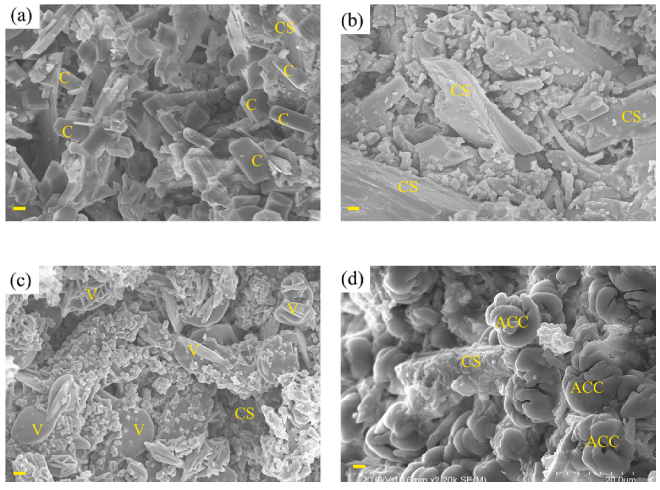

Fig. 4. SEM images showing the microstructure of carbonated wollastonite composites (a) control, (b) with 0.25 M L-Arg, (c) with 0.25 M L-Ser, and (d) with 0.25 M L- Asp. The scale bar shows a 2 μm distance (C: calcite, CS: wollastonite, V: vaterite, ACC: amorphous $CaCO_3$).

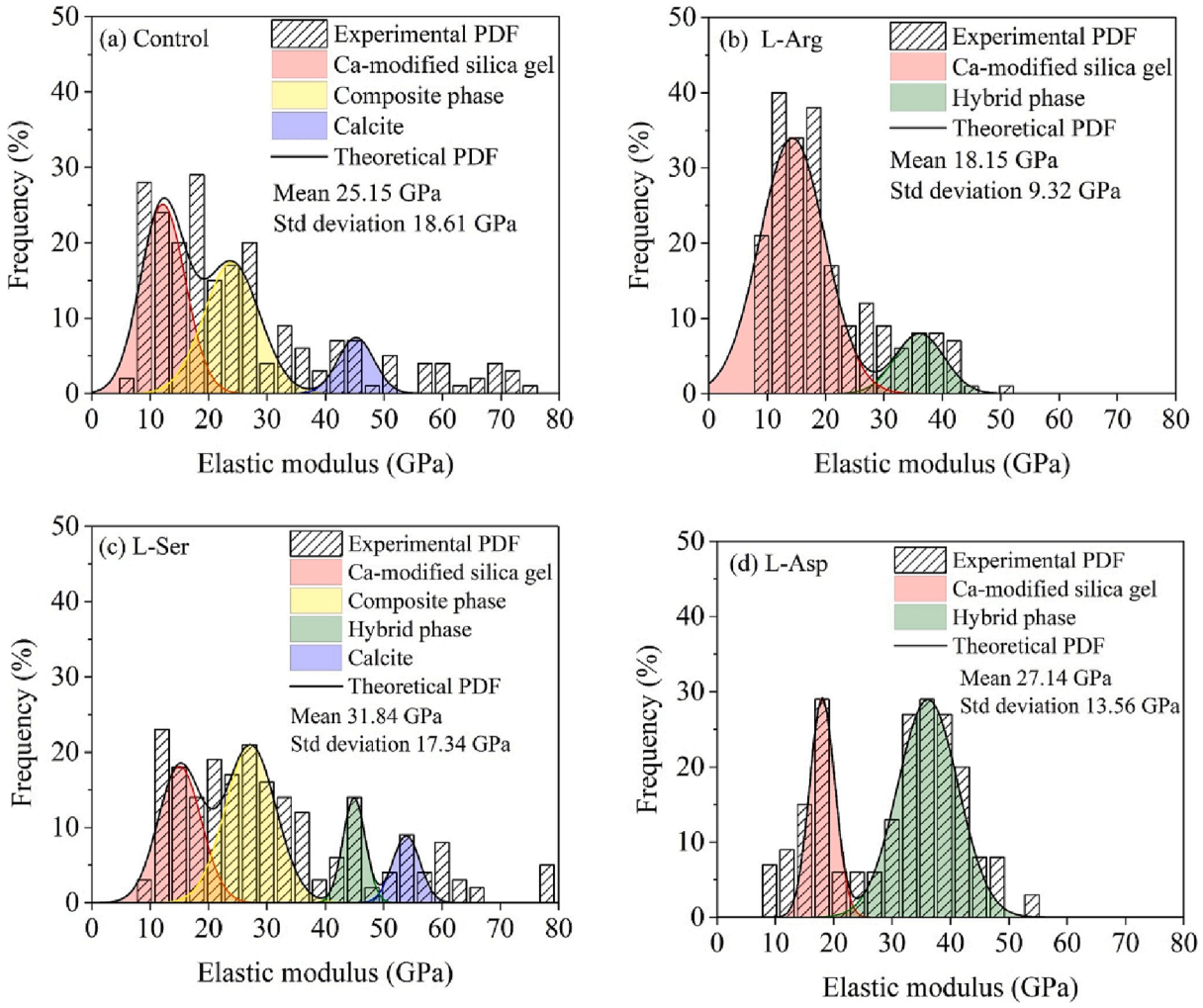

Fig. 5. Frequency distribution plot of elastic modulus for (a) control, (b) L-Arg, (c) L-Ser and (d) L-Asp paste samples.

was observed that the Ca-modified silica gel, composite phase, and the calcite had mean elastic modulus of 12.2 GPa, 23.9 GPa and 45.2 GPa, which is similar to the previous studies [65]. The elastic modulus of the unreacted phases (more than 60 GPa) was not taken into consideration. The composite phases included the Ca-modified silica gel with the calcium carbonate polymorphs. The previous study [66] showed that the mean elastic modulus of pure metastable calcium carbonate (aragonite, vaterite) are in the range of 15–35 GPa. Therefore, the formation of vaterite in amino acid containing batches was expected to reduce the elastic modulus compared to the control batch (containing calcite). Contradictorily, an amino acid containing batches, especially L-Asp and L-Ser batches, showed higher mean modulus compared to that of the control batch. Specifically, in the case of L-Asp containing batch, a significantly higher amount of phase with modulus ranging from 30 to 50 GPa was observed (Fig. 5 (d)). We suggest that this increase in the elastic modulus in amino acid containing batch compared to the pure vaterite (15 ~ 35 GPa) or calcite (control batch, ~ 45 GPa) is due to the formation of organic–inorganic hybrid phase. Worthy to note, the formation of such organic (amino acids) – inorganic (calcium carbonate) is one of the primary mechanisms of stabilizing typical metastable $CaCO_3$ (i.e., vaterite, ACC) during the biomineralization process. Based on a previous study [32], the formation of such organic–inorganic hybrid phase was attributed to the increased flexural strength (106 % higher compared to the control) of the carbonated wollastonite composites. Findings from this work confirm that the enhancement of the mechanical properties of the carbonated wollastonite composite due to the addition of amino acids is valid at the microscale too.

3.2. Macroscale effects of amino acids

3.2.1. Effects of amino acids on the ion leaching and polymorphic change of carbonated matrixes

This experiment aimed to understand how amino acids stabilized polymorphs of $CaCO_3$; and affected the leaching of ions from the carbonated matrixes. The higher amount of Ca^{2+} leaching indicates the dissolution of the binding phases (here $CaCO_3$ and Ca-modified silica gel) and increases the porosity of the matrix [31,53]. Hence, it could eventually reduce the strength of the matrix. According to Mech et al. [31], the amount of calcium ion diffusion depends on the chemical bond of calcium to other minerals in the solid matrix. Other studies claimed that the paste microstructure and pore size refinement, rather than the matrix's calcium content, is mostly responsible for the resistance to leaching [37–39]. Further, the solubility limits for different polymorphs of $CaCO_3$ are different [48], and thus, it could result in a variable leaching rate of Ca^{2+} and Si^{2+} ions from the carbonated matrixes.

Fig. 6 (a) represents the amounts of Ca^{2+} leached out from the carbonated wollastonite matrixes with time. The lowest amount of Ca^{2+} leaching was observed for the matrix containing L-Arg. On the other hand, carbonated wollastonite with L-Asp showed the highest leaching rate of Ca^{2+} ions. The leaching rate of Ca^{2+} ions from carbonated wollastonite was below 20 mg per liter for L-Arg, L-Ser, and control batches after 48 h. On the other hand, L-Asp leached 24 mg of Ca^{2+} per

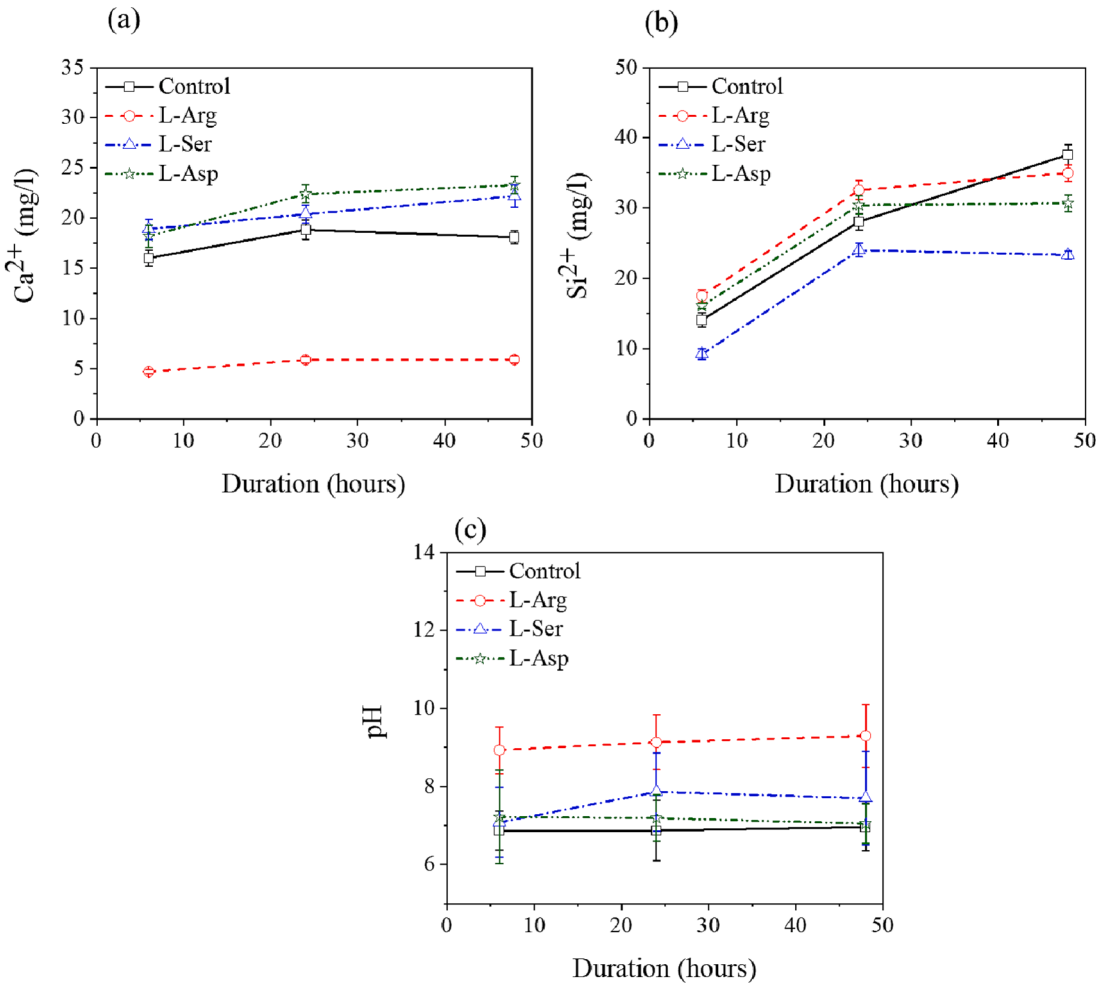

Fig. 6. Ionic concentration of (a) Ca^{2+}, (b) Si^{2+}, and (c) pH of the solutions with soaking durations.

liter of water after 48 h of soaking, indicating a relatively higher rate of $CaCO_3$ dissolution in this matrix. Carbonated wollastonite combined with L-Arg leached more Si^{2+}, and L-Ser leached less Si^{2+} over time, as shown in Fig. 6 (b). For all batches, Si^{2+} leaching was less than 40 mg/l. Further study needs to be conducted to understand better this leaching behavior of amino acids containing carbonated composites.

Fig. 6(c) indicates the pH variability over time of various amino acids combined with wollastonite. Among all amino acids combined with wollastonite batches, L-Arg has the highest pH, and L-Asp has the lowest pH. Higher pH in pore solution reduces the leaching of ions [67]. Due to the higher pH in L-Arg containing carbonated matrix, Ca^{2+} ion leaching was low. According to Luo et al., calcium aspartate could be formed in the presence of L-Asp, which lowers the pH by reducing the ion concentration [68]. Traditional hydrated OPC-based concrete has a pH at around 13 [69]. Higher pH is needed to create a passivation layer that helps prevent the reinforcement's corrosion under the concrete [70]. Lower pH breaks through the passivation layer and initiates corrosion [71]. A pH of more than 9.4 is required for the stabilization of the passivation layer on reinforcement in concrete [72]. However, the pH of the carbonated matrixes are expected to be lower because of the absence of $Ca(OH)_2$ and other alkali hydroxides in this system. Thus, in general, reinforcement in carbonated matrixes is more prone to corrosion compared to the traditional Portland cement [73,74]. Having a higher pH of 9.3, as in the case of L-Arg batch, is a promising indication that after adequate modification of $CaCO_3$ polymorphs, it may be possible to maintain a high pH in the carbonated matrix and thus, lowering the corrosion potential in this system.

The soaked samples were kept in the vacuum desiccator for 24 h for drying. The dried samples were ground using a mortar and pestle. The TGA and FTIR tests of ground samples were performed to check any alternation of $CaCO_3$ polymorphs due to soaking at 60 °C.

TGA results of the ground samples stored in the vacuum chamber after soaking in deionized water are shown in Fig. 7. The calculation procedure for the relative proportion of metastable $CaCO_3$ and $CaCO_3$ content (%) was discussed in Section 2.3.1. Carbonated wollastonite with L-Asp acid has a higher amount of $mCaCO_3$ (Fig. 7(a)), and $CaCO_3$ without amino acid has less amount of $mCaCO_3$ [32]. It was also revealed that there was no significant change in the metastable $CaCO_3$ regardless of leaching. It can be inferred that there was no morphological change due to leaching. There was no significant change in the content of $CaCO_3$ (% by weight), as shown in Fig. 7(b), after soaking in deionized water.

The FTIR spectra of carbonated wollastonite before and after moisture exposure are shown in Fig. 8. $CaCO_3$ polymorphs can be identified from the distinct peaks of FTIR spectra. Doubly generated planner bending vibration ν_4 at frequencies 712 cm^{-1} and out of plane bending ν_2 at frequencies 872 cm^{-1} are typical calcite peaks [75,76]. This acute calcite peak ν_4 was observed in the control batch, and L-Arg, L-Ser containing carbonated wollastonite batches. This peak was not present in L-Asp-containing wollastonite batch, indicating the absence of calcite in the sample (Fig. 8(d)). The ν_2 peak at wavenumber 872 cm^{-1} was observed in all the batches. The ν_2 bending vibration at 856 cm^{-1} is the characteristic aragonite peak [77]. This peak was apparent for the batch-containing L-Ser (Fig. 8(c)), indicating $mCaCO_3$ in this batch. Sharp

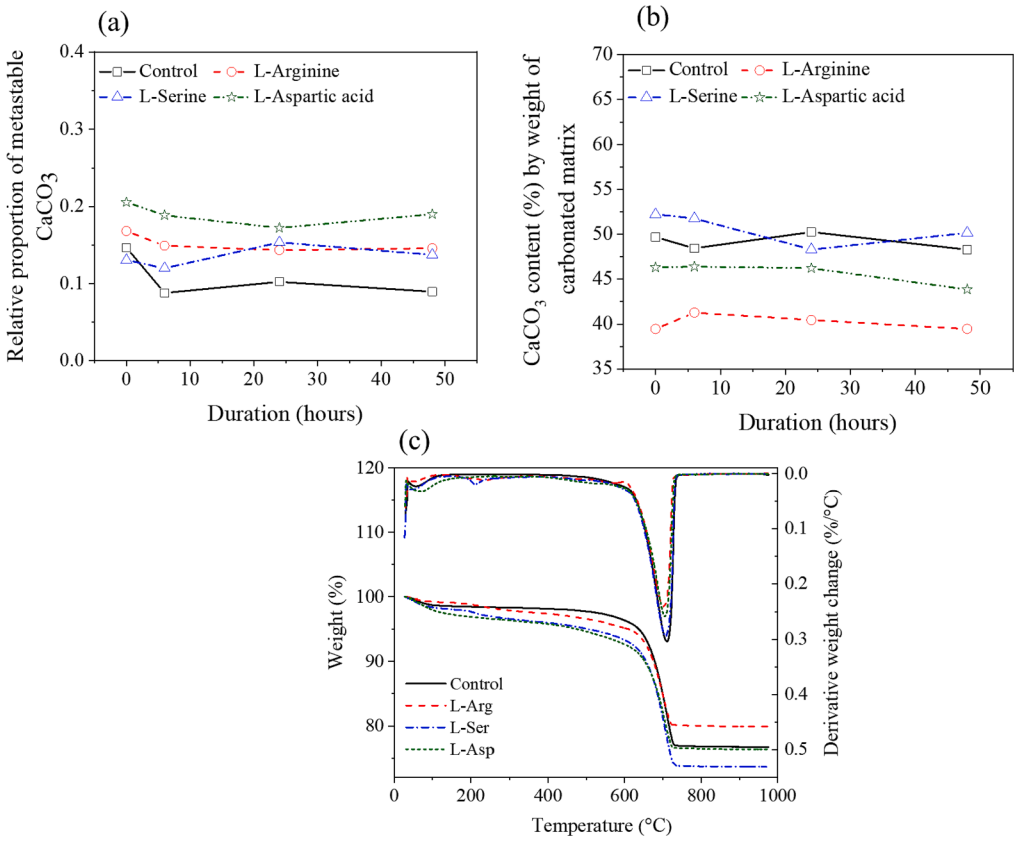

Fig. 7. Thermogravimetric analysis (TGA) of carbonated composites after moisture exposure: (a) relative proportions of metastable $CaCO_3$ with soaking duration, (b) $CaCO_3$ content (%) by weight of carbonated matrix with soaking duration, (c) Thermogravimetric plots of paste samples of 48 h soaking.

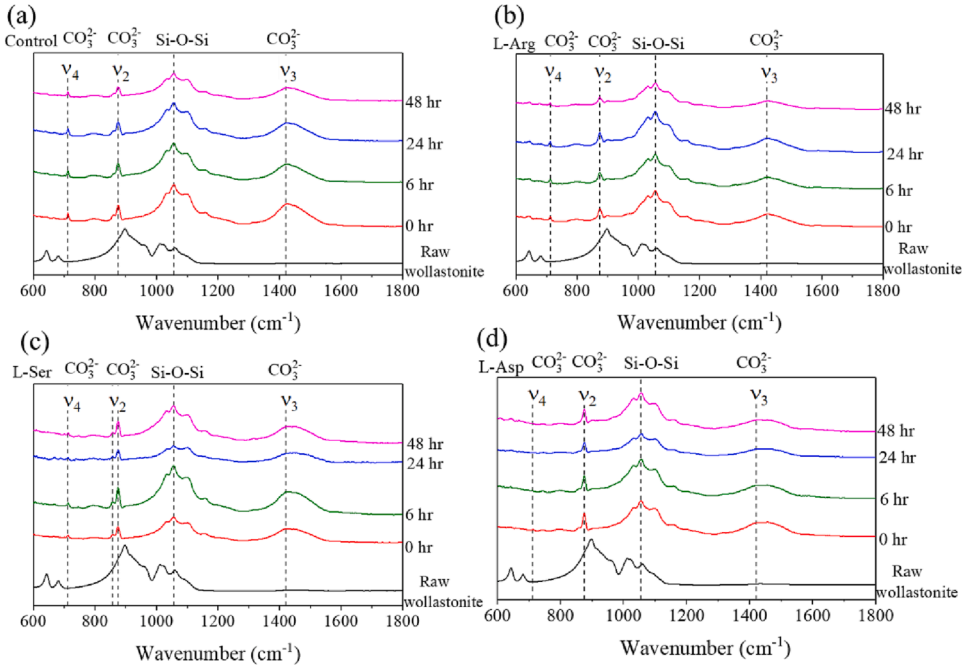

Fig. 8. FTIR normalized plots of carbonation cured wollastonite: (a) control, (b) with L-Arg, (c) with L-Ser, and (d) with L-Asp acid. 0 h indicates the FTIR spectra of wollastonite sample carbonated for 145 h. 6 h, 14 h, and 48 h represent the moisture exposure durations of the carbonated wollastonite composites.

antisymmetric stretching ν_3 at about 1420 cm^{-1} is the distinctive peak for calcite, and a broad antisymmetric stretching ν_3 around this wavenumber is the characteristic peak for ACC [78]. The control batch has a sharp peak at this wavenumber, indicating the formation of calcite (Fig. 8(a)). In the case of amino acid-containing batches, this ν_3 stretching peak was broad, indicating the formation of ACC. Asymmetrical stretching vibration at approximately 1100 cm^{-1} and 1200 cm^{-1} wavenumbers showed the formation of silica gel polymerization [79].

The $mCaCO_3$ phases formed at the early stages are known to instantaneously convert to calcite via solid-state conversion when exposed to water. Accordingly, the moisture exposure experiment was performed in this study to investigate the stability of $mCaCO_3$ formed in the carbonated wollastonite composites due to the presence of amino acids. As observed in Fig. 8, there were no significant changes in the $CaCO_3$ polymorphs present in the carbonated composites due to the moisture exposure. As shown in Fig. 8(b), no change in $CaCO_3$ polymorphism was observed except for a decrease in calcite peak intensity at 712 cm^{-1} (ν_4 vibration) for L-Arg containing carbonated wollastonite. Fig. 8(c) and (d) presented the results of carbonated wollastonite with L-Ser and L-Asp, respectively. There were no changes in $CaCO_3$ polymorphs due to the leaching of ions in both cases. This also supports the TGA results shown in Fig. 7(b). Hence, overall, it could be concluded that the metastable $CaCO_3$ that is stabilized using amino acids remains stable after exposure to water for a longer duration (in this study, 48 h). In another study, we preserved our amino acids containing carbonated samples in the lab (25 °C) condition for two years and found that the morphology didn't change.

3.2.2. Fracture toughness

In a prior investigation, we revealed the impact of amino acids on the compressive and flexural strengths of carbonated composites [32] According to the investigation results, carbonated wollastonite's flexural and compressive strengths increased by 106 % and 48 %, respectively, as their amino acid concentration increased. Notably, the batch containing L-Asp exhibited more consistent compressive and flexural strengths with a reduced standard deviation, which was attributable to the production of consistent spherical ACC in the matrix. In the current study, we investigated the fracture toughness of the amino acids containing carbonated wollastonite composites.

Fracture toughness is a cracking resistance capability used to analyze the fracture behavior of quasi-brittle materials [80]. To determine Mode I fracture toughness, a three-point bending test with a notched beam specimen was performed [81,82]. The addition of amino acids reduces the critical pore size (maximum intensity pore size) in the carbonated wollastonite matrix, as reported in [32]. According to Hu et al., pore size distribution influences the cement paste matrix's strength, permeability, volume change, and toughness [83]. Therefore, the addition of amino acids improves the carbonated system's mechanical performance and toughness.

Fig. 9(a) shows the results of effective critical crack length, a_c. Here all materials have almost similar a_c which indicates that all materials have the same crack initiation energy. The higher amount of metastable $CaCO_3$ ($mCaCO_3$), amino acid-containing carbonated wollastonite has higher fracture energy (G_f) than the control batch. The fracture toughness of carbonated wollastonite containing L-Arg, L-Ser, and L-Asp acids is 32 %, 48 %, and 156 % higher than the control batch. Three to four sample sets were carbonated and analyzed to validate and diminish the uncertainty of the results. Higher fracture energy represents the higher energy required to propagate the crack. The toughness of a composite material also depends on the material characteristic ahead of the crack tip [84], the degree of crystallinity, and the crystal size of the matrix [85]. Additionally, Deshmane et al. postulated that higher crystallinity reduces the toughness of $CaCO_3$ matrix [86]. Accordingly, the higher fracture energy of L-Aspartic containing batch could be due to the presence of lower crystalline $CaCO_3$ in the composite. Fig. 10 shows that amino acid-containing wollastonite batches exhibit higher ductility than the control batch, as demonstrated by the higher maximum CMOD.

4. Conclusions

This article presented a bio-inspired approach to control the $CaCO_3$ crystallization in carbonated cementitious systems using amino acids. The following concluding remarks can be made from this study:

The carbonation rate decreased with amino acid addition in the carbonated wollastonite matrix. Moreover, the higher dosage of amino acids resulted in a slower carbonation rate.

It was demonstrated through SEM images that metastable forms of $CaCO_3$ were obtained with the addition of amino acids. The observed phases were dependent on the alkyl chain length of amino acids.

Nanoindentations revealed that the mean moduli of the carbonated composite containing L-Asp and L-Ser were higher than the control batch. Such enhanced nano-scale elastic modulus was attributed due to the organic–inorganic hybrid phase formation in the presence of amino acids.

The leaching of Ca^{2+} ions from the carbonated matrix was increased due to the amino acids addition. However, the effects of such leaching on the total amount of $CaCO_3$ and its polymorphs were not noticeable.

No polymorphic change of $CaCO_3$ was noticed after moisture exposure, which indicates the higher durability of this organic–inorganic hybrid system.

Amino acids increased the pH of the carbonated matrix. L-Arg with carbonated wollastonite has a pH of 9.3. Therefore, adding selected amino acids can be useful in stabilizing the passivation layer on the reinforcements present in carbonated concrete, thus making these reinforcements less vulnerable to corrosion.

L-Asp acid-containing carbonated calcium silicate has 156 % higher fracture energy than the control batch. This increased toughness was attributed to the potential formation of organic–inorganic hybrid phases as those generally found in biomineral.

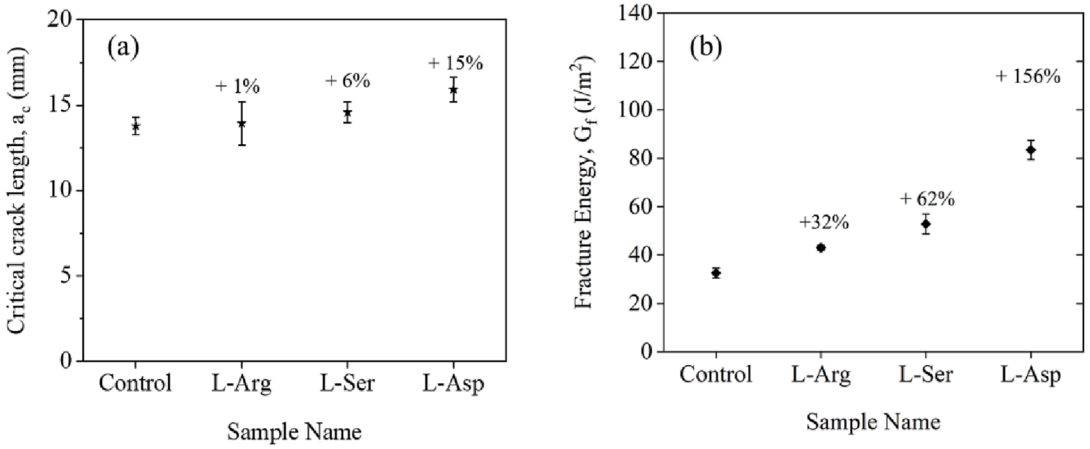

Fig. 9. (a) Critical crack length, and (b) Fracture energy of carbonated wollastonite composites with amino acids (0.25 M).

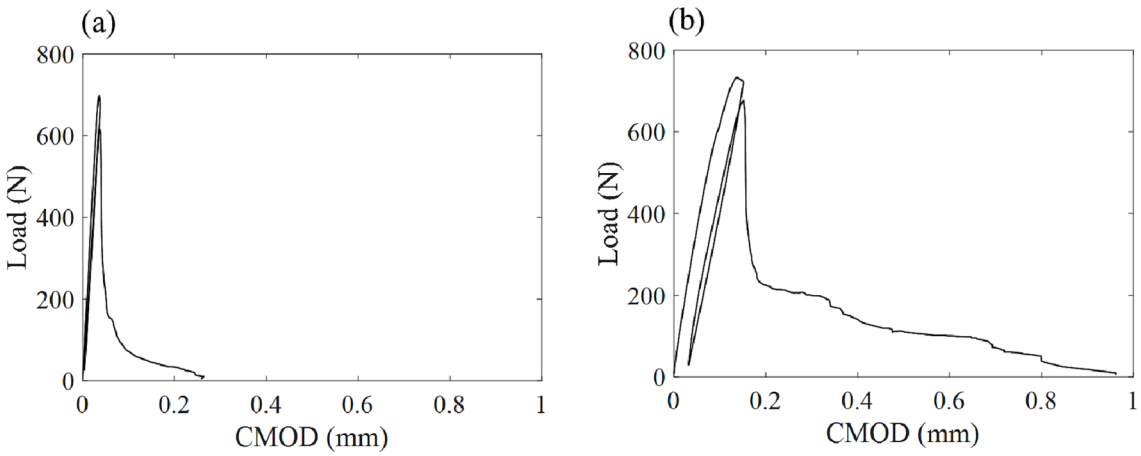

Fig. 10. Load with crack mouth opening displacement (CMOD) plot, (a) without amino acid, and (b) L-Aspartic acid (0.25 M) containing wollastonite.

CRediT authorship contribution statement

Rakibul I. Khan: Conceptualization, Data curation, Formal analysis, Investigation, Writing – original draft, Writing – review & editing. **Muhammad Intesarul Haque:** Data curation, Investigation. **Salman Siddique:** Writing – review & editing. **Eric N. Landis:** Supervision, Writing – review & editing. **Warda Ashraf:** Conceptualization, Formal analysis, Investigation, Funding acquisition, Supervision, Writing – review & editing.

Declaration of Competing Interest

The authors declare that they have no known competing financial interests or personal relationships that could have appeared to influence the work reported in this paper.

Data availability

Data will be made available on request.

Acknowledgment

Funding for this research was provided by the US National Science Foundation (NSF # ECI - 2028462). All opinions, findings, and conclusions or recommendations expressed in this material are those of the authors and do not necessarily reflect the views of the funding agencies.

Appendix A. Supplementary data

Supplementary data to this article can be found online at https://doi.org/10.1016/j.conbuildmat.2023.130816.

References

[1] L. Shen, T. Gao, J. Zhao, L. Wang, L. Wang, L. Liu, F. Chen, J. Xue, Factory-level measurements on CO 2 emission factors of cement production in China, Renew. Sustain. Energy Rev. 34 (2014) 337–349, https://doi.org/10.1016/j.rser.2014.03.025.
[2] W. Ashraf, J. Olek, S. Sahu, Phase evolution and strength development during carbonation of low-lime calcium silicate cement (CSC), Constr. Build. Mater. 210 (2019) 473–482, https://doi.org/10.1016/j.conbuildmat.2019.03.038.
[3] U.S. energy-related carbon dioxide emissions fell in 2019, mainly in electric generation - Today in Energy - U.S. Energy Information Administration (EIA), https://www.eia.gov/todayinenergy/detail.php?id=45836 (accessed October 22, 2021).
[4] E. Assessment. Trends in global CO2 and total greenhouse gas 2020 report, 2020 https://www.pbl.nl/en/publications/trends-in-global-co2-and-total-greenhouse-gas-emissions-2020-report#:~:text=Trends%20in%20Global%20CO2%20and%20Total%20Greenhouse%20Gas%20Emissions%3B%202020%20Report,-21%2D12%2D2020&text=Global%20greenhouse%20gas%20(GHG)%20emissions,2.6%25%2C%20on%20average).
[5] G.L. Golewski, Effect of curing time on the fracture toughness of fly ash concrete composites, Compos. Struct. 185 (2018) 105–112, https://doi.org/10.1016/j.compstruct.2017.10.090.
[6] P.K. Mehta, Greening of the Concrete Industry for Sustainable Development, Concr. Int. 24 (2002) 23–28.
[7] M.C.G. Juenger, F. Winnefeld, J.L. Provis, J.H. Ideker, Advances in alternative cementitious binders, Cem. Concr. Res. 41 (2011) 1232–1243, https://doi.org/10.1016/j.cemconres.2010.11.012.
[8] J.K. Hicks, M.A. Caldarone, E. Bescher, Opportunities from Alternative Cementitious Materials, Concr. Int. 37 (2015) 47–51.
[9] K. Il Song, J.K. Song, B.Y. Lee, K.H. Yang, Carbonation characteristics of alkali-activated blast-furnace slag mortar, Adv. Mater. Sci. Eng. (2014 (2014).), https://doi.org/10.1155/2014/326458.
[10] M.J. Tapas, K. Vessalas, P. Thomas, V. Sirivivatnanon, P. Kidd, Mechanistic Role of Supplementary Cementitious Materials (SCMs) in Alkali-Silica Reaction (ASR), Mitigation (2019) 1–7.
[11] N.R. Rakhimova, R.Z. Rakhimov, Characterisation of ground hydrated Portland cement-based mortar as an additive to alkali-activated slag cement, Cem. Concr. Compos. 57 (2014) 55–63, https://doi.org/10.1016/j.cemconcomp.2014.11.012.
[12] C. Shi, B. Qu, J.L. Provis, Recent progress in low-carbon binders, Cem. Concr. Res. 122 (2019) 227–250, https://doi.org/10.1016/j.cemconres.2019.05.009.
[13] W. Ashraf, I.B. Borno, R.I. Khan, S. Siddique, M.I. Haque, A. Tahsin, Mimicking the Cementation Mechanism of Ancient Roman Seawater Concrete using Calcined Clays, Appl. Clay Sci. 230 (2022), https://doi.org/10.1016/j.clay.2022.106696.
[14] R.I. Khan, S. Siddique, W. Ashraf, Effects of magnesia in semi-hydraulic and non-hydraulic calcium silicate binders during carbonation curing, Constr. Build. Mater. 338 (2022), https://doi.org/10.1016/j.conbuildmat.2022.127628.
[15] M. Abdel Wahab, I. Abdel Latif, M. Kohail, A. Almasry, The use of Wollastonite to enhance the mechanical properties of mortar mixes, Constr. Build. Mater. 152 (2017) 304–309, https://doi.org/10.1016/j.conbuildmat.2017.07.005.
[16] W. Ashraf, J. Olek, N. Tian, Multiscale characterization of carbonated wollastonite paste and application of homogenization schemes to predict its effective elastic modulus, Cem. Concr. Compos. 72 (2016) 284–298, https://doi.org/10.1016/j.cemconcomp.2016.05.023.
[17] R.I. Khan, W. Ashraf, Effects of ground wollastonite on cement hydration kinetics and strength development, Constr. Build. Mater. 218 (2019) 150–161, https://doi.org/10.1016/j.conbuildmat.2019.05.061.
[18] P. Laniesse, C. Cau, D. Coumes, A. Poulesquen, A. Bourchy, A. Mesbah, G. Le, P. Gaveau, C. Cau Dit Coumes, A. Poulesquen, A. Bourchy, A. Mesbah, G. Le Saout, P. Gaveau, C. Cau, D. Coumes, A. Poulesquen, A. Bourchy, A. Mesbah, G. Le, P. Gaveau, Setting and hardening process of a wollastonite-based brushite cement, Cement and Concrete Research. 106 (2018) 65–76. https://doi.org/10.1016/j.cemconres.2018.01.019.
[19] P. Laniesse, C. Cau, D. Coumes, A. Poulesquen, A. Bourchy, A. Mesbah, G. Le, P. Gaveau, Setting and hardening process of a wollastonite-based brushite cement, Cem. Concr. Res. 106 (2018) 65–76, https://doi.org/10.1016/j.cemconres.2018.01.019.
[20] K. Svensson, A. Neumann, F.F. Menezes, C. Lempp, H. Pöllmann, Carbonation of natural wollastonite at non-ambient conditions relevant for CCS-the possible use as cementitious material in wellbores, Applied Sciences (Switzerland). 9 (2019), https://doi.org/10.3390/app9061259.
[21] X. Gao, A. Zhang, S. Li, B. Sun, L. Zhang, The resistance to high temperature of magnesia phosphate cement paste containing wollastonite, Materials and Structures/Materiaux et, Constructions 49 (2016) 3423–3434, https://doi.org/10.1617/s11527-015-0729-9.
[22] G.D.R.N. Ransinchung, B. Kumar, Investigations on Pastes and Mortars of Ordinary Portland Cement Admixed with Wollastonite and Microsilica, J. Mater. Civ. Eng. 22 (2010) 305–313, https://doi.org/10.1061/(ASCE)MT.1943-5533.0000019.
[23] Z. He, A. Shen, Z. Lyu, Y. Li, H. Wu, W. Wang, Effect of wollastonite microfibers as cement replacement on the properties of cementitious composites: A review,

Constr. Build. Mater. 261 (2020), https://doi.org/10.1016/j.conbuildmat.2020.119920.
[24] N.I. Demidenko, L.I. Podzorova, V.S. Rozanova, V.A. Skorokhodov, (A REVIEW), 58 (2001) 308–311.
[25] W. Ashraf, J. Olek, V. Atakan, Carbonation reaction kinetics, CO2 sequestration capacity, and microstructure of hydraulic and non-hydraulic cementitious binders, Sustainable Construction Materials and Technologies. 2016-Augus (2016).
[26] R.I. Khan, M.I. Haque, W. Ashraf, S. Shah, Role of biopolymers in enhancing multiscale characteristics of carbonation-cured cementitious composites, Cem. Concr. Compos. 134 (2022), https://doi.org/10.1016/j.cemconcomp.2022.104766.
[27] P. Wan, J. Hu, W. Ma, L. Wang, L. Cao, H. Tong, Control over the crystal phase, shape, size and aggregation of calcium carbonate via a l-aspartic acid inducing process, Biomaterials 25 (2003) 3923–3929, https://doi.org/10.1016/j.biomaterials.2003.10.038.
[28] Z. Zou, L. Bertinetti, Y. Politi, P. Fratzl, W.J.E.M. Habraken, Control of Polymorph Selection in Amorphous Calcium Carbonate Crystallization by Poly(Aspartic Acid): Two Different Mechanisms, Small 13 (2017) 1–11, https://doi.org/10.1002/smll.201603100.
[29] P. De Silva, L. Bucea, D.R. Moorehead, V. Sirivivatnanon, Carbonate binders: Reaction kinetics, strength and microstructure, Cem. Concr. Compos. 28 (2006) 613–620, https://doi.org/10.1016/j.cemconcomp.2006.03.004.
[30] W. Ashraf, J. Olek, Carbonation activated binders from pure calcium silicates: Reaction kinetics and performance controlling factors, Cem. Concr. Compos. 93 (2018) 85–98, https://doi.org/10.1016/j.cemconcomp.2018.07.004.
[31] P. De Silva, L. Bucea, D.R. Moorehead, V. Sirivivatnanon, Carbonate binders: Reaction kinetics, strength and microstructure, Cem. Concr. Compos. 28 (2006) 613–620, https://doi.org/10.1016/j.cemconcomp.2006.03.004.
[32] R.I. Khan, W. Ashraf, J. Olek, Amino acids as performance-controlling additives in carbonation-activated cementitious materials, Cem. Concr. Res. 147 (2021) 1–39, https://doi.org/10.1016/j.cemconres.2021.106501.
[33] L. Štajner, J. Kontrec, B. Njegić Džakula, N. Maltar-Strmečki, M. Plodinec, D. M. Lyons, D. Kralj, The effect of different amino acids on spontaneous precipitation of calcium carbonate polymorphs, J. Cryst. Growth 486 (2018) 71–81, https://doi.org/10.1016/j.jcrysgro.2018.01.023.
[34] Z. Zou, L. Bertinetti, Y. Politi, P. Fratzl, W.J.E.M. Habraken, Control of Polymorph Selection in Amorphous Calcium Carbonate Crystallization by Poly(Aspartic Acid): Two Different Mechanisms, Small 13 (2017) 1–11, https://doi.org/10.1002/smll.201603100.
[35] J.J. Gaitero, I. Campillo, A. Guerrero, Reduction of the calcium leaching rate of cement paste by addition of silica nanoparticles, Cem. Concr. Res. 38 (2008) 1112–1118, https://doi.org/10.1016/j.cemconres.2008.03.021.
[36] J.E. Mech, Abstract Poro-Damage Approach Applied to Hydro-Fracture Analysis of C oncrete Show Re ferences © 2007 American Society of Civil Engineers, 9399 (2016) 9399. https://doi.org/10.1061/(ASCE)0733-9399(2000)126.
[37] J. Li, Q. Jin, W. Zhang, C. Li, P.J.M. Monteiro, Microstructure and durability performance of sustainable cementitious composites containing high-volume regenerative biosilica, Resour. Conserv. Recycl. 178 (2022), https://doi.org/10.1016/j.resconrec.2021.106038.
[38] A. Kasha, H. Al-Hashim, W. Abdallah, R. Taherian, B. Sauerer, Effect of Ca2+, Mg2 + and SO42- ions on the zeta potential of calcite and dolomite particles aged with stearic acid, Colloids Surf A Physicochem Eng Asp 482 (2015) 290–299, https://doi.org/10.1016/j.colsurfa.2015.05.043.
[39] H. Zhao, Y. Park, D.H. Lee, A.H.A. Park, Tuning the dissolution kinetics of wollastonite via chelating agents for CO2 sequestration with integrated synthesis of precipitated calcium carbonates, PCCP 15 (2013) 15185–15192, https://doi.org/10.1039/c3cp52459k.
[40] L.N. Plummer, E. Busenberg, The solubilities of calcite, aragonite and vaterite in CO2, Geochim. Cosmochim. Acta 46 (1982) 1011–1040, https://doi.org/10.1016/0016-7037(82)90056-4.
[41] O.E. Meiron, E. Bar-David, E.D. Aflalo, A. Shechter, D. Stepensky, A. Berman, A. Sagi, Solubility and bioavailability of stabilized amorphous calcium carbonate, Journal of Bone and Mineral, Research 26 (2011) 364–372, https://doi.org/10.1002/jbmr.196.
[42] K. Scrivener, R. Snellings, B. Lothenbach, A Practical Guide to Microstructural Analysis of Cementitious Materials, 2018. https://doi.org/10.1201/b19074.
[43] W. Ashraf, J. Olek, Carbonation activated binders from pure calcium silicates: Reaction kinetics and performance controlling factors, Cem. Concr. Compos. 93 (2018) 85–98, https://doi.org/10.1016/j.cemconcomp.2018.07.004.
[44] P. Sun, J.R. Grace, C.J. Lim, E.J. Anthony, A discrete-pore-size-distribution-based gas – solid model and its application to the CaO + CO 2 reaction, 63 (2008) 57–70. https://doi.org/10.1016/j.ces.2007.08.054.
[45] D. Mess, A.F. Sarofim, J.P. Longwell, Product Layer Diffusion during the Reaction of Calcium Oxide with Carbon Dioxide, 69 (1999) 999–1005. https://doi.org/10.1021/ef980266f.
[46] J. Sun, M.F. Bertos, S.J.R. Simons, Kinetic study of accelerated carbonation of municipal solid waste incinerator air pollution control residues for sequestration of flue gas CO 2, Energy and Environmental, Science 1 (2008) 370–377, https://doi.org/10.1039/b804165m.
[47] M.I. Haque, W. Ashraf, R.I. Khan, S. Shah, A comparative investigation on the effects of nanocellulose from bacteria and plant-based sources for cementitious composites, Cem. Concr. Compos. 125 (2022), https://doi.org/10.1016/j.cemconcomp.2021.104316.
[48] W.C. Oliver, G.M. Pharr, An improved technique for determining hardness and elastic modulus using load and displacement sensing indentation experiments, J. Mater. Res. 7 (1992), https://doi.org/10.1557/jmr.1992.1564.
[49] S.P. Shah, Determination of fracture parameters (K(Formula presented.) and CTODc) of plain concrete using three-point bend tests, Materials and Structures: Matériaux et, Construction 23 (1990) 457–460, https://doi.org/10.1007/BF02472029.
[50] Y. Jenq, S.P. Shah, Two parameter fracture model for concrete, J. Eng. Mech. 111 (1985) 1227–1241, https://doi.org/10.1061/(ASCE)0733-9399(1985)111:10(1227).
[51] L. Ma, J. Zhu, M. Cui, L. Huang, Y. Su, Biomimetic synthesis of novel calcium carbonate heterogeneous dendrites, New J. Chem. 39 (2015) 5309–5315, https://doi.org/10.1039/c5nj00219b.
[52] K. Maruyama, T. Yoshino, H. Kagi, Synthesizing a composite material of amorphous calcium carbonate and aspartic acid, Mater. Lett. 65 (2011) 179–181, https://doi.org/10.1016/j.matlet.2010.09.039.
[53] P. Wan, J. Hu, W. Ma, L. Wang, L. Cao, H. Tong, Control over the crystal phase, shape, size and aggregation of calcium carbonate via a l-aspartic acid inducing process, Biomaterials 25 (2003) 3923–3929, https://doi.org/10.1016/j.biomaterials.2003.10.038.
[54] L. Štajner, J. Kontrec, B. Njegić Džakula, N. Maltar-Strmečki, M. Plodinec, D. M. Lyons, D. Kralj, The effect of different amino acids on spontaneous precipitation of calcium carbonate polymorphs, J. Cryst. Growth 486 (2018) 71–81, https://doi.org/10.1016/j.jcrysgro.2018.01.023.
[55] W. Ashraf, J. Olek, Carbonation behavior of hydraulic and non-hydraulic calcium silicates: potential of utilizing low-lime calcium silicates in cement-based materials, J. Mater. Sci. 51 (2016) 6173–6191, https://doi.org/10.1007/s10853-016-9909-4.
[56] S. Zhang, Z. Ghouleh, J. Liu, Y. Shao, Converting ladle slag into high-strength cementing material by flue gas carbonation at different temperatures, Resour. Conserv. Recycl. 174 (2021), https://doi.org/10.1016/j.resconrec.2021.105819.
[57] A.E. Morandeau, C.E. White, Role of Magnesium-Stabilized Amorphous Calcium Carbonate in Mitigating the Extent of Carbonation in Alkali-Activated Slag, Chem. Mater. 27 (2015) 6625–6634, https://doi.org/10.1021/acs.chemmater.5b02382.
[58] M. Saharay, A.O. Yazaydin, R.J. Kirkpatrick, Dehydration-induced amorphous phases of calcium carbonate, J. Phys. Chem. B 117 (2013) 3328–3336, https://doi.org/10.1021/jp308353t.
[59] D.J. Tobler, J.D.R. Blanco, K. Dideriksen, K.K. Sand, N. Bovet, L.G. Benning, S.L. S. Stipp, The Effect of Aspartic Acid and Glycine on Amorphous Calcium Carbonate (ACC) Structure, Stability and Crystallization, Procedia Earth and Planetary, Science 10 (2014) 143–148, https://doi.org/10.1016/j.proeps.2014.08.047.
[60] W. Chuajiw, K. Takatori, T. Igarashi, H. Hara, Y. Fukushima, The influence of aliphatic amines, diamines, and amino acids on the polymorph of calcium carbonate precipitated by the introduction of carbon dioxide gas into calcium hydroxide aqueous suspensions, J. Cryst. Growth 386 (2014) 119–127, https://doi.org/10.1016/j.jcrysgro.2013.10.009.
[61] A. Kumar, T. Oey, G. Falzone, J. Huang, M. Bauchy, M. Balonis, N. Neithalath, J. Bullard, G. Sant, The filler effect: The influence of filler content and type on the hydration rate of tricalcium silicate, J. Am. Ceram. Soc. 100 (2017) 3316–3328, https://doi.org/10.1111/jace.14859.
[62] A. Burgos-Cara, C.V. Putnis, C. Rodriguez-Navarro, E. Ruiz-Agudo, Hydration effects on the stability of calcium carbonate pre-nucleation species, Minerals. 7 (2017) 1–15, https://doi.org/10.3390/min7070126.
[63] R.P. Sangodkar, B.J. Smith, D. Gajan, A.J. Rossini, L.R. Roberts, G.P. Funkhouser, A. Lesage, L. Emsley, B.F. Chmelka, Influences of Dilute Organic Adsorbates on the Hydration of Low-Surface-Area Silicates, J. Am. Chem. Soc. 137 (2015) 8096–8112, https://doi.org/10.1021/jacs.5b00622.
[64] W. Chuajiw, K. Takatori, T. Igarashi, H. Hara, Y. Fukushima, The influence of aliphatic amines, diamines, and amino acids on the polymorph of calcium carbonate precipitated by the introduction of carbon dioxide gas into calcium hydroxide aqueous suspensions, J. Cryst. Growth 386 (2014) 119–127, https://doi.org/10.1016/j.jcrysgro.2013.10.009.
[65] W. Ashraf, J. Olek, J. Jain, Microscopic features of non-hydraulic calcium silicate cement paste and mortar, Cem. Concr. Res. 100 (2017) 361–372, https://doi.org/10.1016/j.cemconres.2017.07.001.
[66] R. Ševčík, P. Šašek, A. Viani, Physical and nanomechanical properties of the synthetic anhydrous crystalline CaCO3 polymorphs: vaterite, aragonite and calcite, J. Mater. Sci. 53 (2018), https://doi.org/10.1007/s10853-017-1884-x.
[67] T. Van Gerven, G. Cornelis, E. Vandoren, C. Vandecasteele, Effects of carbonation and leaching on porosity in cement-bound waste, Waste Manag. 27 (2007) 977–985, https://doi.org/10.1016/j.wasman.2006.05.008.
[68] J. Luo, F. Kong, X. Ma, Role of Aspartic Acid in the Synthesis of Spherical Vaterite by the Ca(OH) 2 -CO 2 Reaction, Crystal Growth and Design. 16 (2016) 728–736, https://doi.org/10.1021/acs.cgd.5b01333.
[69] Stover's LLC, No Title, (n.d.).
[70] P. Garcés, P. Saura, E. Zornoza, C. Andrade, Influence of pH on the nitrite corrosion inhibition of reinforcing steel in simulated concrete pore solution, Corros. Sci. 53 (2011) 3991–4000, https://doi.org/10.1016/j.corsci.2011.08.002.
[71] P. Garcés, P. Saura, E. Zornoza, C. Andrade, Influence of pH on the nitrite corrosion inhibition of reinforcing steel in simulated concrete pore solution, Corros. Sci. 53 (2011) 3991–4000, https://doi.org/10.1016/j.corsci.2011.08.002.
[72] B. Huet, L. Hostis, H. Idrissi, Electrochemical behavior of mild steel in concrete : Influence of pH and carbonate content of concrete pore solution, 51 (2005) 172–180. https://doi.org/10.1016/j.electacta.2005.04.014.
[73] M. Moreno, W. Morris, M.G. Alvarez, G.S. Duffó, Corrosion of reinforcing steel in simulated concrete pore solutions effect of carbonation and chloride content, Corros. Sci. 46 (2004) 2681–2699, https://doi.org/10.1016/j.corsci.2004.03.013.

[74] B. Šavija, M. Luković, Carbonation of cement paste: Understanding, challenges, and opportunities, Constr. Build. Mater. 117 (2016) 285–301, https://doi.org/10.1016/j.conbuildmat.2016.04.138.
[75] C.E. Weir, E.R. Lippincott, Infrared studies of aragonite, calcite, and vaterite type structures in the borates, carbonates, and nitrates, Journal of Research of the National Bureau of Standards Section A: Physics and Chemistry. 65A (1961) 173, https://doi.org/10.6028/jres.065a.021.
[76] D. Chakrabarty, S. Mahapatra, Aragonite crystals with unconventional morphologies, J. Mater. Chem. 9 (1999) 2953–2957, https://doi.org/10.1039/a905407c.
[77] C.E. Weir, E.R. Lippincott, Infrared studies of aragonite, calcite, and vaterite type structures in the borates, carbonates, and nitrates, Journal of Research of the National Bureau of Standards Section A: Physics and Chemistry. 65A (1961) 173, https://doi.org/10.6028/jres.065a.021.
[78] M. Sato, S. Matsuda, Structure of vaterite and infrared spectra, Zeitschrift Fur Kristallographie - New Crystal Structures. 129 (1969) 405–410. https://doi.org/10.1524/zkri.1969.129.5-6.405.
[79] W. Ashraf, J. Olek, Carbonation behavior of hydraulic and non-hydraulic calcium silicates: potential of utilizing low-lime calcium silicates in cement-based materials, J. Mater. Sci. (2016), https://doi.org/10.1007/s10853-016-9909-4.
[80] J.G.M. van Mier, Fracture Processes of Concrete (2017), https://doi.org/10.1201/b22384.
[81] A. Carpinteri, G. Fortese, C. Ronchei, D. Scorza, S. Vantadori, Mode I fracture toughness of fibre reinforced concrete, Theor. Appl. Fract. Mech. 91 (2017) 66–75, https://doi.org/10.1016/j.tafmec.2017.03.015.
[82] Y. Jenq, S.P. Shah, Two parameter fracture model for concrete, J. Eng. Mech. 111 (1985) 1227–1241, https://doi.org/10.1061/(ASCE)0733-9399(1985)111:10(1227).
[83] Y. Hu, D. Luo, P. Li, Q. Li, G. Sun, Fracture toughness enhancement of cement paste with multi-walled carbon nanotubes, Constr. Build. Mater. 70 (2014) 332–338, https://doi.org/10.1016/j.conbuildmat.2014.07.077.
[84] C. Chan, J. Wu, J. Li, Y. Cheung, Polypropylene / calcium carbonate nanocomposites, 43 (2002) 2981–2992.
[85] C. Deshmane, Q. Yuan, R.D.K. Misra, On the fracture characteristics of impact tested high density polyethylene-calcium carbonate nanocomposites, Mater. Sci. Eng. A 452–453 (2007) 592–601, https://doi.org/10.1016/j.msea.2006.11.059.
[86] C. Deshmane, Q. Yuan, R.D.K. Misra, On the fracture characteristics of impact tested high density polyethylene-calcium carbonate nanocomposites, Mater. Sci. Eng. A 452–453 (2007) 592–601, https://doi.org/10.1016/j.msea.2006.11.059.